

Revision #1 (6/22/21)

Regular article

Word Count: 5732 up to and including acknowledgments

THERMAL EXPANSION OF MINERALS IN THE AMPHIBOLE SUPERGROUP

Mario Tribaudino

Dipartimento di Scienze Chimiche, della Vita e della Sostenibilità Ambientale

Università di Parma

Viale G.P. Usberti 157/A

I-43100 Parma, Italy

mario.tribaudino@unipr.it

Guy L. Hovis

Department of Geology and Environmental Geosciences, Lafayette College,

Easton, PA 18042

hovisguy@lafayette.edu

Christine Almer

Department of Geology and Environmental Geosciences, Lafayette College,

Easton, PA 18042

christinealmer@gmail.com

Amanda Leaman

Department of Geosciences, Utah State University,

Logan, UT 84322

amanda.leaman3@gmail.com

ABSTRACT

We have investigated the thermal expansion of fifteen naturally occurring chemically diverse amphiboles utilizing high-temperature X-ray powder diffraction data. As done in the first paper of this series on pyroxenes, volume-temperature data were analyzed using the physical Kroll and empirical Fei thermal expansion models. As in pyroxenes, orthorhombic amphibole end members expand more than monoclinic ones, which is related to the greater kinking of the chains of tetrahedra permitted by *Pnma* symmetry. In the case of chemically similar phases, increased Al in octahedral cation sites decreases expansion. Although the ranges of thermal expansion coefficients for amphiboles and pyroxenes are similar, expansion patterns are not the same. Amphiboles exhibit higher expansion along a^* , but lower along b , just the reverse of that observed in pyroxenes. An exception to this are the data for pargasite, which show higher expansion along the b axis due to the presence Al in tetrahedral sites. Current data will be useful in modelling reactions involving amphiboles in both metamorphic and igneous environments.

Keywords: amphiboles, thermal expansion, modeling

INTRODUCTION

In a recent paper, Hovis and others (2021) have reported thermal expansion results for a chemically diverse group of pyroxene minerals based on high-temperature X-ray powder diffraction data. In addition to thermal expansion comparisons within the pyroxene group, the new data, along with previously published results of other investigators, were utilized to examine a wide variety of thermal expansion models based on volumes ranging upward from temperatures (T) near absolute zero (and pressure of 1 bar) to those extending into metamorphic

and igneous regimes. As a follow-on to our previous work on the pyroxene system, we now present data on the thermal expansion of fifteen chemically diverse amphiboles.

The overall goal of our research has been to determine how chemical composition within various mineral groups affects thermal expansion. In order to do so, we have studied compositionally diverse groups of minerals in the garnet, olivine, pyroxene, amphibole, and tourmaline supergroups.

The fundamental structural element of an amphibole, shown in Figure 1, is a double tetrahedral chain that parallels the c crystallographic axis. The latter is in essence a pyroxene single chain bonded to a second chain that is a mirror reflection of the first. Chain orientation and repetition within a single unit cell is like that of pyroxenes, but chain-width doubling results in a doubled b axis. In a structure hierarchical approach (Day and Hawthorne 2020) the amphibole double chain is defined as a ribbon, as it is not possible to break the chain by removing a single tetrahedron. The basic unit of the ribbon is made by four tetrahedra, two of which connected with two tetrahedra and the other two with three (${}^2T_2{}^3T_2$ in Day and Hawthorne 2020 notation). A strip of octahedrally coordinated M(1), M(2), and M(3) sites (the C sites) that collectively correspond to the M1 octahedra of pyroxenes, links to ${}^2T_2{}^3T_2$ ribbons in the a- and b-directions. The M(4) sites (also known as B sites) are located along the flanks of the octahedral band, surrounded by 8 oxygens, not all of which are coordinated to the central atom. The A site is located between the back-to-back (as opposed to apical) six-fold tetrahedral rings of the ribbon unit; this typically is occupied by large cations such as Na or K and associated with hydroxyl groups of the so-called W site.

Overall, then, the greater structural complexity of amphiboles relative to pyroxenes correlates with wider chemical variation, as reflected by the general formula $A_{0-1}B_2C_5T_8O_{22}W_2$,

where A = □, Na, K, Ca, Li; B = Ca, Na, Mn²⁺, Fe²⁺, Mg, Li; C = Mg, Fe²⁺, Mn²⁺, Al, Mn³⁺, Fe³⁺, Ti⁴⁺, Li; T = Si, Al, Ti, Be²⁺, and W = OH⁻, F, Cl, O²⁻ (Hawthorne et al., 2012). Together, the structural complexity and extensive chemical substitution (including potential order-disorder phenomena at elevated T) make the modelling of thermal expansion for amphiboles difficult. This is even more exasperated by the difficulties involved in synthesizing some amphibole end members (Maresch and Czank, 2007).

The above factors help explain why comparison of pyroxene and amphibole thermal expansion behavior has been limited. Indeed, in the Holland and Powell (2011) data base thermal expansion coefficients for eight of eleven amphibole end members were estimated. Prior to the investigation of synthetic glaucophane by Jenkins and Corona (2006), the lone amphibole studies were those on tremolite (Sueno et al. 1973) and synthetic K and Na richterite (Cameron et al. 1983). Since 2006, high-temperature studies investigated additional natural and synthetic amphibole specimens (synthetic richterite, Tribaudino et al. 2008; anthophyllite, Welch et al. 2011a; gedrite, Zema et al. 2012; riebeckite, Oberti et al. 2018; pargasite, Comboni et al. 2018; Fe-holmquistite, Oberti et al. 2019). Related studies also have been carried out on the high temperature *P2₁/m - C2/m* phase transition in various amphiboles (Yang and Hirschmann 1995; Reece et al 2000; Iezzi et al. 2005, 2011; Camara et al 2003, 2008). With the main foci on crystal structure changes at high temperature, cation ordering and deprotonation, however, thermal expansion data in such studies have generally been given as an auxiliary result. Moreover, in studies involving phase transitions, the major interest has been on modelling transition behavior rather than thermal expansion.

In the current paper, we shall examine the thermal expansion of a number of natural amphiboles, most having close-to-end-member compositions. The aim is to provide further data

for thermodynamic modelling of metamorphic and igneous assemblages where amphiboles are major phases, to look at general trends with composition and structure, and to compare data on amphiboles with those recently reported for compositionally analogous pyroxenes (Hovis et al. 2021). Amphibole unit-cell volumes have been fit to the same models as in the companion pyroxene paper, that is, the Kroll physical (Kroll et al. 2012) and Fei empirical (1995) formulations.

SAMPLES AND METHODS

Amphibole samples investigated

The amphibole mineral supergroup comprises a large number of end members, the classification of which has been discussed by Hawthorne et al. (2012). For current work we chose to perform X-ray powder diffraction measurements only on naturally occurring amphibole specimens for which chemical analyses were available (Table 1). Overall, a total of four orthoamphiboles and eleven clinoamphiboles were investigated. Orthoamphiboles include two anthophyllite specimens having different Mg:Fe ratios, plus gedrite and holmquistite. Clinoamphiboles include cummingtonite, grunerite, two tremolite samples, ferro-actinolite, pargasite, hastingsite, richterite, glaucophane, and riebeckite. Crystallographic, chemical, and other information pertaining to these samples are recorded in Table 1; the calculated partitioning comes from the software of Locock (2014), which was used to convert oxide-based chemical analyses. The site occupancies recorded in Table 1 were determined on the assumption that $(\text{OH}, \text{F}, \text{Cl}) = 2 - 2\text{Ti}$ pfu, and therefore, $^{\text{W}}\text{O} = 2\text{Ti}$, retaining where present the FeO/Fe₂O₃ partitioning based on wet chemical or Mössbauer analysis. The naming of the amphiboles was done using the program AMPH2012 (Oberti et al 2012).

Samples for this study were obtained from the U.S. National Museum of Natural History (NMNH), the American Museum of Natural History (AMNH), M. Darby Dyar, and David Jenkins. Despite its label, NMNH R14496 "edenite" was actually found to be tremolite based on microprobe analysis on record at NMNH, even though the sample comes from the type locality (Edenville, NY) for edenite. This specimen shall hereafter be referred to as Edenville tremolite.

Methods

X-ray powder diffraction measurements were conducted from room T to ~928 °C at mostly 50 °C intervals on a PANalytical Empyrean X-ray powder diffraction system equipped with an Anton-Parr HTK 1200N heating stage. Actual sample temperatures were checked through independent experiments on several compounds that display second-order phase transitions, as described in detail by Hovis et al. (2021). Generally, it was found that the observed temperatures of our experiments were 16 °C to 28 °C above the set temperature displayed on the controller console. The latter range in temperature correction probably does not represent real variation in instrumental vs. actual T over time, but likely reflects the standard deviation in average ΔT values that became evident only after ever-increasing experience with the new XRD system over an extended period of time. During data reduction, unit-cell calculations utilized adjusted amphibole peak positions that employed NIST (NBS) 640a silicon as an internal standard; extended discussion of this methodology is given in the pyroxene paper (Hovis et al. 2021).

Generally, unit-cell dimensions were calculated using the X-ray software of Holland and Redfern (1997). To avoid automated indexing of low-intensity X-ray peaks related to phase impurities, the *hkl* identities of all peaks were assigned manually, for which both the American

Mineralogist Crystal Structure Database (Downs and Hall-Wallace, 2003) and PANalytical Database were invaluable. Because of this manual indexing, rather than automated indexing now available on various XRD systems, we regard the stated standard deviations of our computed unit-cell dimensions to be realistic. The wavelength of Cu K α 1 radiation for all calculations was taken to be 1.540598 Å.

Our calculated unit-cell dimensions for all amphiboles are presented in Table S1, which also includes post-heating room-T unit-cell dimensions for tremolite. Reported standard deviations from the Holland software represent 1 σ values; these should be multiplied by a factor of 2 or 3 to obtain a more realistic estimate of data uncertainty.

RESULTS

Fitting of the data

Valid thermal expansion data require that the analyzed phase not change in chemical composition or cation distribution during heating. Amphiboles are particularly prone to such changes at high T. The latter may include (1) oxidation (as observed in pyroxenes by Hovis et al. 2021), (2) deprotonation (Welch et al. 2007), and (3) cation exchange among M(1), M(2), and M(3) sites, also between M(4) and A sites. In fact, ten of the fifteen investigated samples did indeed show evidence of iron oxidation by changed sample color to brown, red-brown, or red by the conclusion of their XRD experiments. Of the remaining five samples, two showed breakdown to pyroxenes plus other phases based on post-run room-T XRD measurements and phase identification.

What we assume to be deprotonation similar to that observed for riebeckite by Oberti et al. (2018) was indicated by off-trend unit-cell dimensions as f(T) for multiple samples. **Plots of**

the c unit-cell parameter against T were found to be especially good indicators of sample breakdown (see supplementary Figure S1). These typically show a dampening of the rate of increase in c with T , or even an outright decrease with increasing T , as samples deteriorate. Breakdown is especially evident for hastingsite, pargasite, cummingtonite, grunerite, riebeckite, glaucophane, and holmquistite, but shown by additional samples as well. It is noteworthy that our proposed T for the beginning of breakdown of riebeckite agrees with that of Oberti et al. (ibid). Although off-trend data points were not utilized in the analysis of thermal expansion data, a portion of such unused high- T data has been included and shown in red in supplementary Table S1, which will give the reader a feeling for the subtleties of sample behavior at elevated T .

Only two samples showed no obvious evidence of sample deterioration up to the highest T of our experiments, namely tremolite NMNH 144178 and Edenville tremolite NMNH R14496. The Edenville sample, however, does show a significant difference beyond combined error in room- T volumes measured pre- vs. post-heating. Note that in analysing the data for tremolite we have included the 140 K data of Yang and Evans (1996). We also have fit data for the entire T range (110 to 900 K) for synthetic richterite from a study (Tribaudino et al. 2008) that utilized a sample composition [$^A\text{Na}_{0.87}^B(\text{Na}_{0.87}\text{Ca}_{1.03}\text{Mg}_{0.09})^C\text{Mg}_{5.00}^T\text{Si}_{8.00}\text{O}_{22}(\text{OH})_2$], which lacked elements susceptible to oxidation and avoided the potential for cation exchange among M(1), M(2) and M(3) sites, all filled by the same cation.

Fits have been done according to the physical model of Kroll and the empirical model of Fei using the EOSfit7 package of Angel et al. (2014). Details on the equations and different merits of the models are discussed in Hovis et al. (2021). In the Kroll physical equation we can independently refine the (1) volume thermal expansion, (2) unit-cell volume at the reference temperature (which here is room temperature), (3) first derivative of the bulk modulus (K') and

(4) Debye temperature. However, the various parameters are highly correlated; most critical is the deviation from linear behavior of volume with temperature, something that requires low temperature data, preferably as close as possible to 0 K. This has been done for plagioclase and jadeite pyroxene (Tribaudino et al 2011, Hovis et al. 2021), and in the case of amphiboles for synthetic richterite (Tribaudino et al. 2008). If only data above room temperature are available, both K' and the Debye temperature must be fixed. This is important for present data, where in most cases datasets range only to a few hundred degrees. As a result, we have used K' and Debye temperature simply as fitting parameters within the range of reasonable physical values. The K' bulk modulus derivative has a value of 4 fitting unit-cell volume vs. pressure in a Birch-Murnaghan second order equation of state (Angel 2001). Expanding to a third order Birch-Murnaghan (BM) allows refinement of K' , generally to higher values, indicating greater curvature in a V vs. P plot. For amphiboles, using a third order BM equation of state, Nestola et al. (2012) found K' to be 6.2(2) for a gedrite crystal. Welch et al. (2011b), on the other hand, obtained a K' value of 11 for anthophyllite. Using these values in fitting present high- T data, however, gave invariably higher V vs. T curvature than observed experimentally, whereas $K'=4$ resulted in better agreement. In the case of pyroxenes, we observed better fits constraining the experimental K' from 4 in jadeite to 8 in enstatite. As shown in Figure 2, comparing compositionally analogous orthoamphibole (anthophyllite) and pyroxene (enstatite), we see that the latter shows greater curvature in V - T relations.

In giving a reasonable value for the Debye temperature, it is noted that, except for tremolite, the Debye temperature obtained from amphibole entropy data in Holland et al. (2011) is linearly related to unit-cell volume according to the equation (unit cell doubled for monoclinic members)

$$1) \theta_D = 1965(204) - 0.86(11)V_{298}$$

It is this expression that was used to retrieve the Debye temperatures from the room-temperature volumes for present amphiboles. The lone exception to this derivation is for tremolite, whose data are inconsistent with equation 1 and whose Debye temperature was obtained directly from that reported in the Holland et al. (2011) data base.

The empirical Fei equation given below allows fitting of thermal expansion data without any assumption on parameters:

$$(2) V = V_0 \exp(a_0(T - T_{ref}) + 1/2a_1(T^2 - T_{ref}^2) - a_2(1/T - 1/T_{ref}))$$

Here V_0 is the unit-cell volume at the reference temperature, and a_0 , a_1 and a_2 are empirical parameters. It was possible to obtain all four parameters only for tremolite, as for most amphiboles the a_2 and sometimes also the a_1 could not be refined with errors lower than the obtained value. If the Fei equation is truncated to the square term, variation of thermal expansion with temperature changes linearly. If the square term is also dropped, thermal expansion becomes constant with temperature. In either case the model is physically inconsistent, but both are useful for fitting the data.

Tables 2 and 3 show the results of fitting data using both Kroll and Fei models. Figure 3 shows thermal expansion coefficients at 298 K according to both models. Fei-based thermal expansion is generally greater than that for the Kroll model. This likely results from data for several amphiboles for which it was necessary to truncate the Fei plot after the first term, giving only a linear V-T fit, which results in overestimation of thermal expansion at room temperature. The relatively high Debye temperature, well above room temperature, indicates that for amphiboles we are far from saturation in thermal expansion at room temperature, and that constant thermal expansion is an unphysical approximation.

DISCUSSION

Thermal expansion systematics and comparison with pyroxenes.

Comparing the thermal expansion of amphiboles obtained with the Kroll and Fei models, we observe that, no matter the model, orthoamphiboles show greater expansion than clin amphiboles, except for Li-bearing holmquistite (Figs 3 and 4). Among the monoclinic amphiboles, cummingtonite and the sodic amphiboles riebeckite and glaucophane show the lowest expansion, whereas tremolite, richterite and Al-bearing amphiboles pargasite and hastingsite show similar thermal expansion, between 2.5 and $2.7 \cdot 10^{-5}/\text{K}$. Differences between this and previous investigations are limited except for the synthetic glaucophane of Jenkins and Corona (2006), which shows thermal expansion well below that of any other amphibole. Comparing the thermal expansion of amphiboles classified by the same name, we observe a systematically lower thermal expansion for specimens having higher contents of trivalent cations in the C sites (Fig. 5), confirming what was observed for synthetic glaucophane by Jenkins and Corona (2006). This accounts as well for differences between sodic and calcic amphiboles, as the former contain more Al and Fe^{3+} exchanging with R^{2+} cations in the C sites, as an effect of Na-for-Ca exchange. The same is found in pyroxenes with the substitution of a divalent cation with Al, as thermal expansion decreases from diopside to jadeite (Cameron et al. 1973; Tribaudino et al. 2008, Pandolfo et al. 2015) and from diopside to Ca-Tschermak (Hovis et al. 2021), with Fe^{3+} substitution into diopside toward aegirine (Cameron et al. 1973, Tribaudino et al. 2008), and with trivalent Cr^{3+} substitution (Tribaudino et al. 2005) (Table S1). Generally, then, thermal expansion is decreased with the entrance of trivalent cations into the ribbon of octahedra in the amphibole structure.

Even so, the added complexity of structure and chemical variability of amphiboles in comparison with pyroxenes provides some results that at first view seem surprising. For example, chemically distinct amphiboles such as tremolite and pargasite have almost the same thermal expansion, despite the Al content of the latter. Yet tremolite and cummingtonite, neither of which contain Al, show distinctly different thermal expansion values. This is likely due to the different Ca content in tremolite and cummingtonite. How, then, might one think about the comparative systematics of thermal expansion in these systems? Some clue may come from a comparison with pyroxenes.

Figure 6 shows the volume thermal expansion for both amphiboles and pyroxenes. Note that for pyroxenes we present the data discussed in Hovis et al. (2021) plus additional literature data that has been refined using the Kroll equation (Fig. 6, Table S1). A first observation is that amphiboles and pyroxenes do have similar thermal expansion and volume. The apparent higher frequency of pyroxenes with lower thermal expansion in Fig. 6 is due to the larger number of sodic pyroxenes sampled, namely four amphiboles with the Na – R³⁺ substitution in the corresponding B and C sites compared with fourteen pyroxenes. Second, orthorhombic pyroxenes and amphiboles show higher thermal expansion than monoclinic ones. Third, thermal expansion for monoclinic pyroxenes is almost linearly related to volume; amphiboles, on the other hand, are scattered. For amphiboles, therefore, volume is not a predictor of thermal expansion. Volume instead depends on chemical substitutions that follow both numerous and complex paths (Hawthorne and Oberti 2007), much more so than is the case for pyroxenes. Sodic amphiboles show higher volume but similar thermal expansion as pyroxenes, where the volume difference is explained simply by C-site coexistence of Al with larger cations like Mg or Fe²⁺. Ideal glaucophane, for example, has 3/5 Mg and 2/5 Al, with a larger average cation size due to

the larger Mg, whereas jadeite has only Al in the M1 site (corresponding to the C site in amphiboles).

One may also compare chemically and structurally related couples of amphiboles and pyroxenes such as tremolite and diopside or anthophyllite and enstatite. Such couples share the same cations in corresponding M2-B, M1-C and T sites, i.e., Ca, Mg and Si for tremolite-diopside and Mg, Mg and Si for anthophyllite-enstatite. At room temperature amphiboles display slightly higher thermal expansion than do the corresponding pyroxenes. For diopside recent determinations by Pandolfo et al. (2015) and Hovis et al. (2021) give similar thermal expansion coefficients of $2.37(2)$ and $2.42(1) \times 10^{-5} \text{ K}^{-1}$ compared with the present value for tremolite of $2.59(2) \times 10^{-5} \text{ K}^{-1}$. The values for anthophyllite by Welch et al. (2011a), $3.22(2) \times 10^{-5} \text{ K}^{-1}$, and present work, $3.10(2) \times 10^{-5} \text{ K}^{-1}$, compare with an enstatite value of $2.62(2) \times 10^{-5} \text{ K}^{-1}$ from Yang and Ghose (1994) and $2.605(5) \times 10^{-5} \text{ K}^{-1}$ from Hovis et al (2021). These differences, however, disappear at higher temperature because of the greater curvature of V-T relations for pyroxenes. Indeed pyroxenes show on average higher Debye temperature than amphiboles, with an average Debye temperature from present amphibole work of 419(45) K compared with 493(44) K for pyroxenes (Hovis et al. 2021). For example, at 800°C diopside shows thermal expansion coefficients of $3.47(3)$ and $3.56(2) \times 10^{-5} \text{ K}^{-1}$ based on the data of Pandolfo et al. (2015) and Hovis et al. (2021), respectively, compared with a value of $3.41(3) \times 10^{-5} \text{ K}^{-1}$ for tremolite. Current values for anthophyllite are $4.12(4)$ and $4.30(2) \times 10^{-5} \text{ K}^{-1}$ relative to those of $4.21(1)$ and $4.25(5) \times 10^{-5} \text{ K}^{-1}$ for enstatite.

Thermal deformation models and comparison with pyroxenes

In order to interpret these results and compare structural changes between pyroxenes and amphiboles, axial thermal expansions have been calculated along the three crystallographic axes in orthorhombic amphiboles, and for the \underline{a}^* , \underline{b} , and \underline{c} directions in monoclinic samples. Such directions provide a crystallographic marker common to both mineral groups. In Fig. 1 the directions are shown in the structure of a monoclinic amphibole. Along \underline{a}^* , the axial expansion α_{a^*} is given by $\alpha_{a^*} = (d_{100,T1} - d_{100,T0}) / [(T1 - T0)d_{100,T0}]$, where d_{100} is the (100) interplanar distance along \underline{a}^* , i.e. $d_{100} = a_0 \sin \beta$, equivalent to a_0 in orthorhombic crystals. Thermal expansion along \underline{a}^* is related to the distance of the facing tetrahedral chains, which make a sheet of alternating up and down chains, corresponding to the displacement of the facing tetrahedral sheets in a direction normal to the (100) crystallographic plane (Fig. 1). Along the \underline{b} and \underline{c} directions axial expansion was calculated as $\alpha_b = (b_{0,T1} - b_{0,T0}) / [(T1 - T0)b_{0,T0}]$ and $\alpha_c = (c_{0,T1} - c_{0,T0}) / [(T1 - T0)c_{0,T0}]$, respectively. Expansion along \underline{b} corresponds to the widening along [010] due to lateral displacement of the tetrahedral chains and of the C and B cations with temperature, whereas the \underline{c} direction is that of tetrahedral ribbon. Kinking due to deformation of the ribbon changes the \underline{c} parameter, noting that tetrahedra are the stiffest polyhedra with increasing temperature. These deformations can easily be compared with those of pyroxenes, where similar crystallographic features are found. In monoclinic pyroxenes the orientation of the \underline{a} axis is different than in monoclinic amphiboles, due to the different setting of the monoclinic cell relative to that in amphiboles (Sueno et al. 1973, Tribaudino et al. 2008), which hinders direct comparison of axial deformation along \underline{a} . On the other hand, the d_{100} accounts for the same interlayer spacing, disregarding that in amphiboles the tetrahedral layer is made by ribbons, and in pyroxenes by chains. The axial expansion of amphiboles is reported in Table 4.

Although amphiboles and pyroxenes show similar volume thermal expansion, axial expansion differs. Amphiboles expand more along the a^* direction, but less along b (Figure 7). Despite some overlap along the b direction, amphiboles generally expand to a greater degree normal to the tetrahedral layer. An exception is pargasite, which shows similar expansion to that in clinopyroxenes, very close to that of Ca-Tschermak pyroxene. Indeed, both have significant entrance of Al in the T sites, up to 25% in pargasite, and 50% in Ca-Tschermak pyroxene. Along the c direction, amphiboles and pyroxenes expand similarly, with more significant differences instead between clino- and ortho- phases.

To compare behavior among amphiboles, we have tested simple bivariate relations among volume or axial thermal expansion and chemical composition. This approach failed to give a correlation higher than $R^2=0.6$, likely due to the complexity of amphibole chemistry. Alternatively, one can use principal components multivariate analysis (PCA, Webb and Briggs 1966), which is useful in finding hidden correlations that may be concealed in the univariate approach. In the present case there are four variables, namely the thermal expansion along the three directions plus the volume thermal expansion, whose variance in our amphiboles can be described by two principal components, each one accounting for a percentage of the global variance. Moreover, the orientation and length of the plot of each of the variables shows the degree of correlation of the variables with respect to the principal components. To do such an analysis we have utilized the PAST software of Hammer et al. (2001), the results of which are discussed next (Fig. 8). In fact, two main components explain 53 and 30% of the global variance.

The PCA plot in Figure 8 shows a scattered distribution of amphiboles, with distinct fields for calcic, sodic, and ortho amphiboles, confirming different behavior with respect to the thermal expansion axes. Calcic amphiboles mostly correlate with a_{22} axial expansion, i.e., with

thermal expansion along the b axis. Among calcic amphiboles, Al-bearing pargasite shows the highest correlation (Fig. 8). Orthoamphiboles are most correlated with expansion along the c axis (a_{33}), with holmquistite closer to cummingtonite and sodic amphiboles. Holmquistite, cummingtonite and sodic amphiboles are in a field with correlation opposite that of calcic amphiboles. An exception is synthetic glaucophane, which apparently does not relate to any other group (Fig. 8). Note that the close relation between a_{33} expansion along the c axis and global thermal expansion indicates that volume thermal expansion correlates with expansion along the c axis. Thus, expansion along c becomes a major factor in explaining differences in thermal expansion.

Additional observations can be made within each amphibole group. For orthoamphiboles, in the cases of anthophyllite and holmquistite $\alpha_a > \alpha_c > \alpha_b$, but in gedrite $\alpha_c > \alpha_a \sim \alpha_b$; note again that gedrite has significant Al in the T sites. For clinoamphiboles, significant differences exist among pargasite, sodic, calcic and cummingtonitic members. In cummingtonite and the sodic amphiboles riebeckite and glaucophane, the axial expansion pattern is $\alpha_{a^*} > \alpha_b > \alpha_c$. In calcic amphiboles tremolite and hastingsite, axial expansion along a is closer to that along b, $\alpha_{a^*} \sim \alpha_b > \alpha_c$, whereas in pargasite $\alpha_b > \alpha_c > \alpha_{a^*}$.

Greater expansion along the c axis, with little difference in other directions, accounts for the higher volume expansion in orthorhombic vs. monoclinic pyroxenes and amphiboles. This is apparently an effect of the different chain configurations in monoclinic and orthorhombic phases, where monoclinic amphiboles and pyroxenes have a $C2/m$ and $C2/c$ structure with only one symmetrically independent crystallographic chain. Expansion along the c axis involves opening the tetrahedral chain by increasing the kinking angle O3-O3-O3 of the chain in pyroxenes and the corresponding O(5)-O(6)-O(5) angle in amphiboles (Fig. 1, Cameron et al. 1973; Sueno et al.

1973). In cummingtonite the transition from $P2_1/m$ to the $C2/m$ structure occurs with large changes in the O(5)-O(6)-O(5) angles, and as a consequence in the c axial parameter (Camara et al 2003). However, ~~but~~ as long as the high temperature monoclinic $C2/m$ structure is attained, the O(5)-O(6)-O(5) angle changes little with temperature. Cummingtonite with $C2/m$ structure, as in the present work, shows an elongated tetrahedral ribbon at room temperature with an O(5)-O(6)-O(5) angle of about 170° (Yang and Hirshmann 1993), i.e., almost fully extended. Natural orthorhombic amphiboles and pyroxenes show respectively $Pnmm$ and $Pbca$ space groups in which there are two non-equivalent A and B tetrahedral chains, as in $P2_1/m$ cummingtonite. One of these is highly kinked and expands to a greater extent with increasing temperature, approaching the value of the other chain. Together with unkinking a higher expansion along the c axis occurs. In anthophyllite Welch et al. (2011a) found that between 25 and 700°C the A and B chains change their kinking angle by 6° and 13° , respectively, and by 700°C assume a fully extended configuration. Yet in monoclinic tremolite and riebeckite Sueno et al. (1973) and Oberti et al. (2018) found that over the same temperature interval the unique chain changes its kinking angle by less than 3° , and the c parameter also changes little. In pyroxenes as well ~~the~~ thermal expansion along c is higher in ortho- than clinopyroxenes, and in low-temperature $P2_1/c$ pigeonite higher than in high temperature $C2/c$ pigeonite (Tribaudino et al. 2002).

In pargasite we find lower expansion along a^* , and higher along b . Expansion along the c axis is lower than that along b , yet pargasite expansion along c is the greatest among monoclinic amphiboles. This trend is similar to that found in Ca-Tschermak pyroxene, which like pargasite has Al in tetrahedral and octahedral sites (Fig. 7). This suggests that the coupled substitution of Al-for-Si in the T sites together with Al-for-(Mg, Fe) in the C sites increases the attraction

between the tetrahedral and octahedral layers, thus hindering expansion along a^* , which is the direction of stacking of the octahedral and tetrahedral layers.

The above description in terms of expansion along the crystallographic axes is useful for a structural interpretation. Yet, in monoclinic amphiboles, the thermal expansion is constrained only by the b crystallographic axis. The two other axes of a thermal expansion ellipsoid lie on the (010) plane at some angle to the a and c axes. Therefore, to correctly describe thermal expansion we need to know the size and orientation of the thermal expansion axes on (010). To make such determinations, thermal expansion ellipsoids were calculated comparing room-temperature and higher-temperature unit-cell data (see Hovis et al. 2021) using the EOSfit7 program (Angel et al. 2014) with Eulerian strain and taking as reference cartesian axes a^* , b and c (Angel et al 2014). The three strain axis orientations are referred to as ϵ_1 , ϵ_2 and ϵ_3 , where ϵ_1 and ϵ_3 are rotated from the a^* and c axial directions, respectively, and ϵ_2 is coincident with b . The range over which the strain and axial expansion were calculated plus the strain scalar and orientation are reported in Table 4.

Such calculations show that for tremolite and richterite the three axes are scaled as $\epsilon_1 \sim \epsilon_b > \epsilon_3$. For cummingtonite and (with a different angle in) sodic amphiboles riebeckite and glaucophane, $\epsilon_1 > \epsilon_b > \epsilon_3$, and for pargasite, $\epsilon_3 \sim \epsilon_b > \epsilon_1$.

Except for pargasite, the direction showing the highest deformation is that closest to a^* . In sodic amphiboles this occurs at angles of 5° and -10° with a^* . In tremolite, cummingtonite and richterite the higher deformation on the (010) plane is at a greater angle to a^* , between a^* and c , and around 20° from a^* . The direction with the least expansion is closer to the c axis, except in pargasite where the higher expansion occurs at angles of 28° and 37° with the c axis. Lastly, note

that in tremolite the direction of deformation changes with temperature, coinciding with the same observation for synthetic richterite (Tribaudino et al., 2008a).

As previously found by Tribaudino et al. (2008a), in calcic amphiboles and cummingtonite the deformation occurs most at an angle between 10 and 30° from a^* , along the direction of the M(4)-O(5) distance, a bond which increases most during heating. The M(4)-O(5) bond corresponds essentially to the M2-O3 distance in calcic pyroxenes. In sodic amphiboles and pyroxenes the same distance changes little, and the deformation is driven by changes in the M1 polyhedron along a direction normal to the c axis (Tribaudino et al. 2008a).

IMPLICATIONS

Amphiboles are widespread in igneous and metamorphic environments (Martin 2007, Schumaker 2007). Once correctly identified and characterized, they can be important indicators of specific tectonic and geodynamic environments. Several reactions involving amphiboles are powerful tools in constraining metamorphic facies. In this context thermal expansion is a key feature. Indeed, volume changes in metamorphic transitions can involve significant quantities of amphibole, for example, in the blueschist and amphibolite facies. Moreover, in describing the rheological properties of rocks, mineral compositions and transformations dictate the volume changes observed at high temperature.

This and other recent investigations raise questions whose solutions will benefit from future amphibole single-crystal studies. Because of the broad chemical and structural variation in this system, further research is needed not only on additional amphibole end members, but also on strategically selected intermediate amphibole compositions. Here we suggested fruitful directions for future high-T single-crystal studies.

One unresolved issue concerns the effect of Al on thermal expansion. Present work indicates that even for amphiboles classified with the same name, the effect of Al substitution can be different from sample to sample. How does Al substitution in the C sites affect thermal expansion, and what are the effects of other cations in the A site relative to Al?

A second issue involves comparison of thermal expansion for glaucophane with that of its pyroxene analogue omphacite. Synthetic vs. natural omphacites show little difference in thermal expansion (Pandolfo et al. 2015). On the other hand, synthetic glaucophane shows a very low thermal expansion, 20 % lower than any of the amphibole and pyroxenes that have been examined. It also shows different orientation of axial thermal deformation. The difference with natural glaucophane can in part be explained by the lower Al content of natural glaucophane, but polysomatic errors also may influence thermal expansion. Further study on synthetic glaucophane - riebeckite synthetic amphiboles may help clarify the effect of chemical variability and/or structural defects on the thermal expansion.

ACKNOWLEDGEMENTS

Conducted at Lafayette College, the high-T X-ray work has involved undergraduate students in both data collection and analysis; indeed, two such students (now graduated) are coauthors of this paper. This research would not have been possible without financial support of the U.S. National Science Foundation via grants EAR-1019809 and EAR-1028953 for both the X-ray equipment and student participation. Samples for this study were obtained from the U. S. National Museum of Natural History (Jeff Post, Paul Powhat) and the American Museum of Natural History (George Harlow). In addition, M. Darby Dyar (Mt. Holyoke College) made available a number of orthoamphiboles studied by Anthony Law (1973, 1981, 1989), also

specimen PBM-10 collected by the late Paul B. Moore. David Jenkins (Binghamton University) provided specimen MS-2825 obtained from the UCLA mineral collection via Bernard Evans. This study could not have been successful without the chemical data so generously provided by these institutions and individuals, including a new microprobe analysis for sample PBM-10 by Molly McCanta (University of Tennessee) in cooperation with Dr. Dyar.

REFERENCES CITED

- Alvaro, M., Angel, R.J., Marciano, C., Milani, S., Scandolo, L., Mazzucchelli, M.L., Zaffiro, G., Rustioni, G., Briccola, M., Domeneghetti, M.C., and Nestola, F. (2015) A new micro-furnace for in situ high-temperature single-crystal X-ray diffraction measurements. *Journal of Applied Crystallography*, 48, 1192-1200.
- Angel, R.J. (2001) Equations of state. In "High-temperature and high-pressure crystal chemistry", R.M. Hazen and R.T. Downs (eds.), *Reviews in Mineralogy and Geochemistry*, 41, 35-60.
- Angel, R.J., Gonzalez-Platas, J., and Alvaro, M. (2014) EosFit7c and a Fortran module (library) for equation of state calculations. *Zeitschrift für Kristallographie - Crystalline Materials*, 229, 405-419.
- Cámara, F., Oberti, R., Iezzi, G., and Della Ventura, G. (2003) The $P2_1/m \leftrightarrow C2/m$ phase transition in synthetic amphibole $\text{Na}(\text{NaMg})\text{Mg}_5\text{Si}_8\text{O}_{22}(\text{OH})_2$: Thermodynamic and crystal-chemical evaluation. *Physics and Chemistry of Minerals*, 30, 570-581.
- Cámara, F., Oberti, R., and Casati, N. (2007) The $P2_1/m \leftrightarrow C2/m$ phase transition in amphiboles: New data on synthetic $\text{Na}(\text{NaMg})\text{Mg}_5\text{Si}_8\text{O}_{22}\text{F}_2$ and the role of differential polyhedral expansion. *Zeitschrift für Kristallographie*, 223, 148-159.

- Cameron, M., Sueno, S., Papike, J.J., and Prewitt, C.T. (1983) High temperature crystal chemistry of K and Na fluor-richterites. *American Mineralogist*, 68, 924-943.
- Cameron, M., Sueno, S., Prewitt, C.T., and Papike, J.J. (1973) High-temperature crystal chemistry of acmite, diopside, jadeite, spodumene and ureyite. *American Mineralogist*, 58, 594-618.
- Comboni, D., Lotti, P., Gatta, G.D., Merlini M., Liermann, H.P., and Frost, D.J. (2018). Pargasite at high pressure and temperature. *Physics and Chemistry of Minerals*, 45, 259-278.
- Downs, R.T., and Hall-Wallace, H. (2003) The American Mineralogist crystal structure database. *American Mineralogist*, 88, 247-250.
- Fabries, J., and Perseil, E.A. (1971) Nouvelles observations sur les amphiboles orthorhombiques. *Bulletin de la Société Française de Minéralogie*, 94, 385-395.
- Ghose, S., (1965) Mg^{2+} - Fe^{2+} order in orthopyroxene, $Mg_{0.93}Fe_{1.07}Si_2O_6$. *Zeitschrift für Kristallographie*, 122, 81-99.
- Fei, Y. (1995) Thermal Expansion. In "A handbook of physical constants, mineral physics and crystallography". Ahrens, J.A. (ed). AGU Reference Shelf, 2, 29-44.
- Finger, L.W., and Ohashi, Y. (1976) The thermal expansion of diopside to 800 °C and a refinement of the crystal structure at 700 °C. *American Mineralogist*, 61, 303-310.
- Goldman, D.S. (1979) A reevaluation of Mössbauer spectroscopy of calcic amphiboles. *American Mineralogist*, 64, 109-118.
- Hammer, Ø., Harper, D.A.T., Ryan, P.D. (2001) PAST: Paleontological statistics software package for education and data analysis. *Palaeontologia Electronica* 4, 9pp.

- Haselton, H.T. Jr., Hemingway, B.S., and Robie, R.A. (1984) Low-temperature heat capacities of $\text{CaAl}_2\text{SiO}_6$ glass and pyroxene and thermal expansion of $\text{CaAl}_2\text{SiO}_6$ pyroxene. American Mineralogist, 69, 481-489.
- Hawthorne, F.C., and Grundy, H.D. (1976) The crystal chemistry of amphiboles: IV. X-ray and neutron refinements of the crystal structure of tremolite. The Canadian Mineralogist, 14, 334-345.
- Hawthorne, F.C., Oberti, R., Harlow, G.E., Maresch, W.V., Martin, R.F., Schumacher, J.C., and Welch, M.D. (2012) Nomenclature of the amphibole supergroup. American Mineralogist, 97, 2031-2048.
- Holland, T.J.B., and Powell, R. (2011) An improved and extended internally-consistent thermodynamic dataset for phases of petrological interest, involving a new equation of state for solids. Journal of Metamorphic Geology, 29, 333-388.
- Holland, T.J.B., and Redfern, S.A.T. (1997) Unit-cell refinement: Changing the dependent variable and use of regression diagnostics. Mineralogical Magazine, 61, 65-77.
- Hovis, G.L., Tribaudino, M., Leaman, A., Almer, C., Altomare, C., Morris, M., Maksymiw, N., Morris, D., Jackson, K., Scott, S., Tomaino, G., and Mantovani, L. (2021) Thermal expansion of minerals in the pyroxene system and examination of various thermal expansion models. American Mineralogist, 106, DOI: <https://doi.org/10.2138/am-2021-7650>.
- Hugh-Jones, D. (1997) Thermal expansion of MgSiO_3 and FeSiO_3 ortho- and clinopyroxenes. American Mineralogist, 82, 689-696.
- Iezzi, G., Tribaudino, M., Della Ventura, G., Nestola, F., and Bellatreccia, F. (2005) High- T phase transition of synthetic $^A\text{Na}^B(\text{LiMg})^C\text{Mg}_5\text{Si}_8\text{O}_{22}(\text{OH})_2$ amphibole: an X-ray

- synchrotron powder diffraction and FTIR spectroscopic study. *Physics and Chemistry of Minerals*, 32, 515-523
- Iezzi, G., Tribaudino, M., Della Ventura, G., and Margiolaki, I. (2011) The high temperature $P2_1/m \rightarrow C2/m$ phase transitions in synthetic amphiboles along the richterite-(BMg)-richterite join. *American Mineralogist*, 96, 353-363.
- Jackson, J.M., Palko, J.W., Andrault, D., Sinogeikin, S.V., Lakshtanov, D.L., Wang, J., Bass, J.D., and Zha, C. (2003) Thermal expansion of natural orthoenstatite to 1473 K. *European Journal of Mineralogy*, 15, 469-473.
- Jenkins, D., and Corona, J.C. (2006) Molar volume and thermal expansion of glaucophane. *Physics and Chemistry of Minerals*, 33, 356-362.
- Kroll, H., Kirfel, A., Heinemann, R., and Barbier, B. (2012) Volume thermal expansion and related thermophysical parameters in the Mg,Fe olivine solid-solution series. *European Journal of Mineralogy*, 24, 935-956.
- Law, A.D. (1973) Critical evaluation of 'statistical best fits' to Mössbauer spectra. *American Mineralogist*, 58, 128-130.
- Law, A.D. (1989) Studies of the orthoamphiboles: IV. Mössbauer spectra of anthophyllites and gedrites. *Mineralogical Magazine*, 53, 181-191.
- Law, A.D., and Whittaker, E.J.W. (1981) Studies of the orthoamphiboles I. The Mössbauer and infrared spectra of holmquistite. *Bulletin de Minéralogie*, 104, 381-386.
- Locock, A.J. (2014) An Excel spreadsheet to classify chemical analyses of amphiboles following the IMA 2012 recommendations. *Computers & Geosciences*, 62, 1-11.

- Maresch, W.V., and Czank, M. (2007) The significance of the reaction path in synthesizing single-phase amphibole of defined composition. *Reviews in Mineralogy and Geochemistry*, 67, 287-322.
- Martin, R.F. (2007) Amphiboles in the igneous environment. *Reviews in Mineralogy and Geochemistry*, 67, 323-358.
- Nestola, F., Pasqual, D., Welch, M.D., and Oberti, R. (2012) The effects of composition upon the high-pressure behaviour of amphiboles: compression of gedrite to 7 GPa and a comparison with anthophyllite and proto-amphibole. *Mineralogical Magazine*, 76, 987-995.
- Oberti, R., Boiocchi, M., Zema, M., Hawthorne, F.C., Redhammer, G.J., Susta, U., and Della Ventura, G. (2018) The high-temperature behaviour of riebeckite: expansivity, deprotonation, selective Fe oxidation and a novel cation disordering scheme for amphiboles. *European Journal of Mineralogy*, 30, 437-449.
- Oberti, R., Boiocchi, M., and Zema, M. (2019) Thermoelasticity, cation exchange, and deprotonation in Fe-rich holmquistite: Toward a crystal-chemical model for the high-temperature behavior of orthorhombic amphiboles. *American Mineralogist*, 104, 1829-1839.
- Pandolfo, F., Cámara, F., Domeneghetti, C.M., Alvaro, M., Nestola, F., Karato, S., and Amulele, G. (2015) Volume thermal expansion along the jadeite-diopside join. *Physics and Chemistry of Minerals*, 42, 1-14.
- Papike, J.J., and Ross, M. (1970) Gedrites: Crystal structures and intracrystalline cation distributions. *American Mineralogist*, 55, 1945-1972.

- Parrish, W. (1953) X-ray reflection angle tables for several standards. Technical Report No. 68, Philips Laboratories Incorporated, Irvington on Hudson, New York.
- Rao, K.S.R., and Rao, A.T. (1981) Pargasite-rich rock from the Eastern Ghats, India. Mineralogical Magazine, 44, 111.
- Reece J.J., Redfern S.A.T., Welch, M.D., and Henderson, C.M.B. (2000) Mn-Mg disordering in cummingtonite: a high temperature neutron powder diffraction study. Mineralogical Magazine, 64, 255-266.
- Robinson, P., and Jaffe, H.W. (1969) Chemographic exploration of amphibole assemblages from central Massachusetts and southwestern New Hampshire. Mineralogical Society of America Special Paper 2, 251-274.
- Schumacher, J.C. (2007) Metamorphic amphiboles: composition and coexistence. Reviews in Mineralogy and Geochemistry, 67, 359-416.
- Shannon, E.V. (1924) An iron amphibole similar to hudsonite from Custer County, Idaho. American Journal of Science, Series 5, 8, 323-324.
- Sueno, S., Cameron, M., Papike, J.J., and Prewitt, C.T. (1973) High temperature crystal chemistry of tremolite. American Mineralogist, 58, 649-664.
- Tilley, C.E. (1957) Paragenesis of anthophyllite and hornblende from the Bancroft area, Ontario. American Mineralogist, 42, 412-416.
- Tribaudino, M., Nestola, F., Cámara, F., and Domeneghetti, M.C. (2002) The high temperature $P2_1/c-C2/c$ phase transition in Fe-free pyroxene ($\text{Ca}_{0.15}\text{Mg}_{1.85}\text{Si}_2\text{O}_6$): structural and thermodynamic behavior. American Mineralogist, 87, 648-657.
- Tribaudino, M., Nestola, F., and Ohashi, H. (2005) High temperature single crystal investigation in a clinopyroxene of composition $(\text{Na}_{0.5}\text{Ca}_{0.5})(\text{Cr}_{0.5}\text{Mg}_{0.5})\text{Si}_2\text{O}_6$. European Journal of

- Mineralogy, 17, 297-304.
- Tribaudino, M., Bruno, M., Iezzi, G., Della Ventura, G., and Margiolaki, I. (2008a) The thermal behavior of richterite. *American Mineralogist*, 93, 1659-1665.
- Tribaudino, M., Nestola, F., Bruno, M., Boffa Ballaran, T., and Liebske, C. (2008b) Thermal expansion along the $\text{NaAlSi}_2\text{O}_6$ - $\text{NaFe}^{3+}\text{Si}_2\text{O}_6$ and $\text{NaAlSi}_2\text{O}_6$ - $\text{CaFe}^{2+}\text{Si}_2\text{O}_6$ solid solutions. *Physics and Chemistry of Minerals*, 35, 241-248.
- Tribaudino, M., Bruno, M., Nestola, F., Pasqual, D., and Angel, R.J. (2011) Thermoelastic and thermodynamic properties of plagioclase feldspars from thermal expansion measurements. *American Mineralogist*, 96, 992-1002.
- von Knorring, O., and Hornung, G. (1961) On the lithium amphibole holmquistite, from Benson pegmatite mine, Mtoko, Southern Rhodesia. *Mineralogical Magazine*, 32, 731-735.
- Webb, W., and Briggs, L. (1966). The Use of Principal Component Analysis to Screen Mineralogical Data. *The Journal of Geology*, 74(5), 716-720.
- Welch, M.D., Camara, F., Della Ventura, G., and Iezzi, G. (2007) Non-ambient in situ studies of amphiboles. *Reviews in Mineralogy and Geochemistry*, 67, 223-260.
- Welch, M.D., Cámara, F., and Oberti, R. (2011a) Thermoelasticity and high-T behaviour of anthophyllite. *Physics and Chemistry of Minerals*, 38, 321-334.
- Welch M. D., Gatta G. D., and Rotiroti N. (2011b) The high-pressure behavior of orthorhombic amphiboles *American Mineralogist*, 96, 623–630.
- Yang, H., and Evans, B.W. (1996) X-ray structure refinement of tremolite at 140 and 295K: Crystal chemistry and petrologic implications. *American Mineralogist*, 81, 1117-1125.

- Yang, H., and Ghose, S. (1994) Thermal Expansion, Debye temperature and Grüneisen parameter of synthetic (Fe, Mg)SiO₃ orthopyroxenes. *Physics and Chemistry of Minerals*, 20, 575-586.
- Yang, H., and Hirschmann, M.M. (1995) Crystal structure of *P*2₁/*m* ferromagnesian amphibole and the role of cation ordering and composition in the *P*2₁/*m*-*C*2/*m* transition in cummingtonite. *American Mineralogist*, 80, 916-922.
- Zema, M., Welch, M.D., and Oberti, R. (2012) High-T behavior of gedrite: Thermoelasticity, cation ordering and dehydrogenation. *Contributions to Mineralogy and Petrology*, 163, 923-937.

TABLES

All Tables submitted as separate files (6/22/21)

Table 1: Chemical and other information for the amphiboles investigated.

Table 2: Volume thermal expansion data (Kroll model).

Table 3: Volume thermal expansion data (Fei model).

Table 4: Axial thermal expansion and components of the strain ellipsoid in amphiboles. The α_{a^*} , α_b and α_c axial expansion correspond to the a_{11} , a_{22} , a_{33} diagonal components of the strain ellipsoid in the Angel et al. (2014) notation. Note that thermal expansion is here obtained from discrete steps between low temperature (LT) and high temperature (HT) unit cells, whereas the volume thermal expansion (Tables 2 and 3) is derived from the model, as a first derivative. The angle between ε_1 and a^* is positive when ε_1 is between a^* and c , negative when between a^* and minus c . Data from 1: this work; 2: Sueno et al. (1973); 3: Comboni et al. (2018); 4: Tribaudino et al. (2008); 5: Oberti et al. (2018); 6: Jenkins and Corona (2006); 7: Welch et al. (2011a); 8: Zema et al. (2012).

Table S1: High temperature unit-cell data (Hovis) *[to be deposited]*

Table S2: Axial and volume thermal expansion of pyroxenes and amphiboles. Volume thermal expansion calculated at $T=298$ K, Kroll model. *[to be deposited]*

FIGURES

Figure captions

Figure 1: Crystal structure of tremolite: along the c axis (above), with a and a^* directions superimposed, and along the b axis (below, left), with the a^* direction dashed, and (below right) showing the double chain with the O(5)-O(6)-O(5) angle; B site in yellow, C sites in orange, green OH- hydroxyls, red oxygen, dashed green indicates the position of the A site

Figure 2: Comparison of thermal expansion for enstatite vs. anthophyllite. Note deviation at higher temperature of the V-T trend for anthophyllite, also the greater curvature of V-T data for enstatite.

Figure 3: Calculated thermal expansion coefficients at 298 K according to the Fei and Kroll models. Cummingtonite collectively refers to cummingtonite and grunerite.

Figure 4: Thermal expansion vs. volume for various amphiboles at room temperature.

Figure 5: Thermal expansion and trivalent content in C sites in amphiboles of the same name (connected by arrows)

Figure 6: Unit-cell volume and thermal expansion in clino- and ortho- pyroxenes and amphiboles. For volume comparison the unit cells of monoclinic amphiboles and orthopyroxenes was halved, and that of orthoamphiboles was divided by four. Data from Table S1.

Figure 7: Axial thermal expansion in clino- and ortho- pyroxenes and amphiboles. Data from Table S2.

Figure 8: Principal Component Analysis (PCA) plot showing the multivariate variation among 21 amphiboles in terms of axial and volume thermal expansion. Vectors indicate the direction and strength of each variable to the overall distribution. Symbols as in figures 3 and 4.

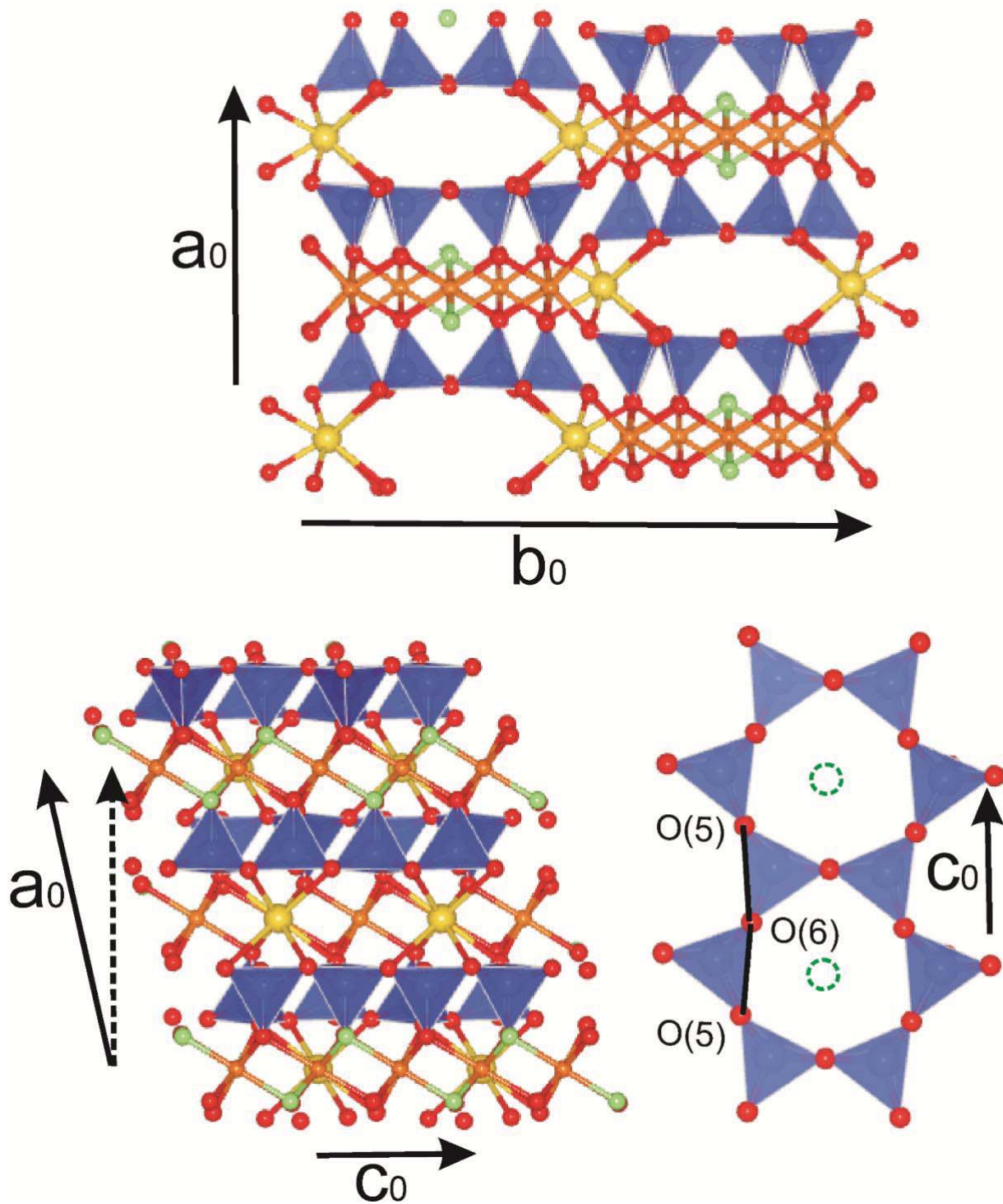


Figure 1

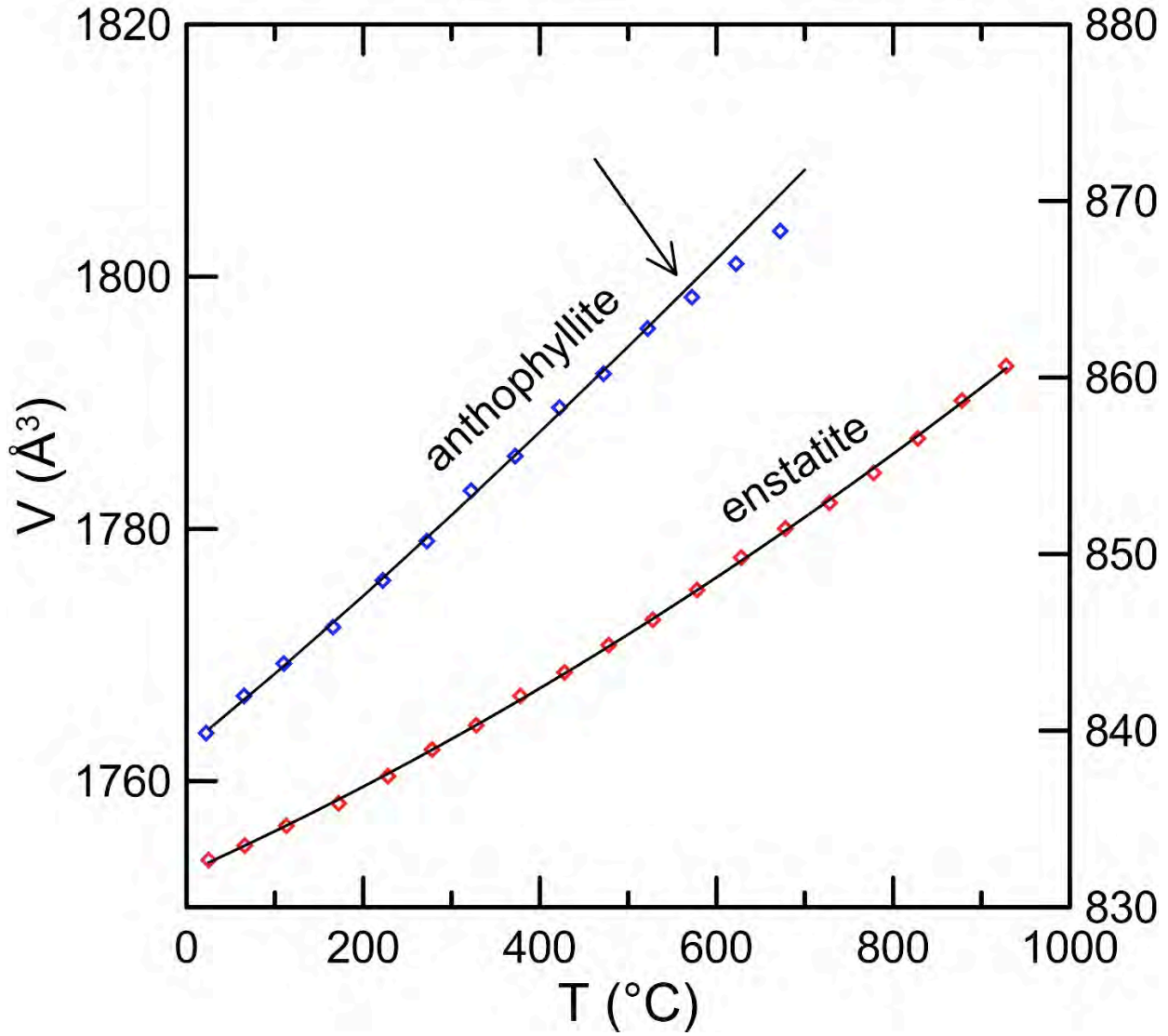


Figure 2

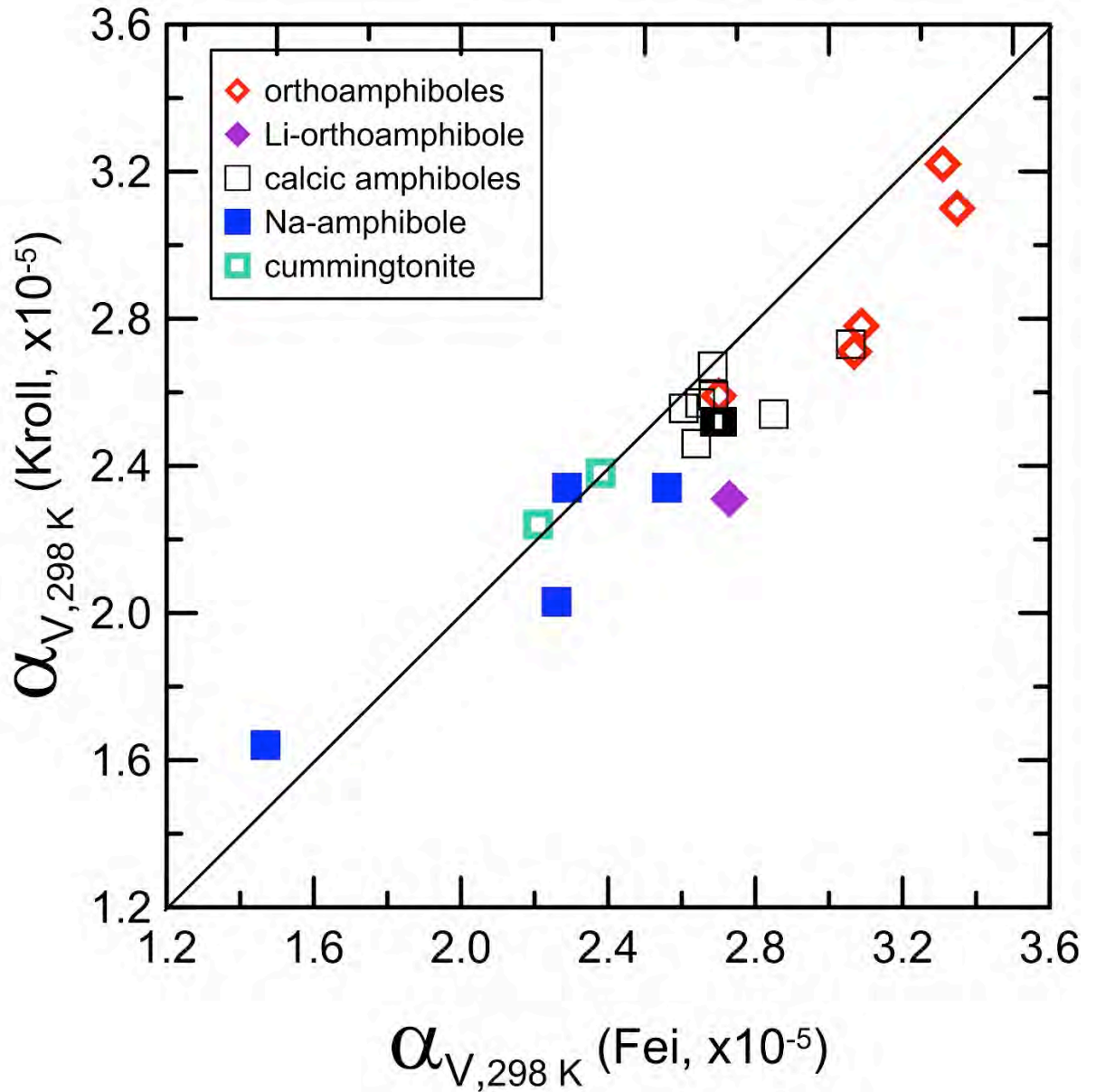


Figure 3

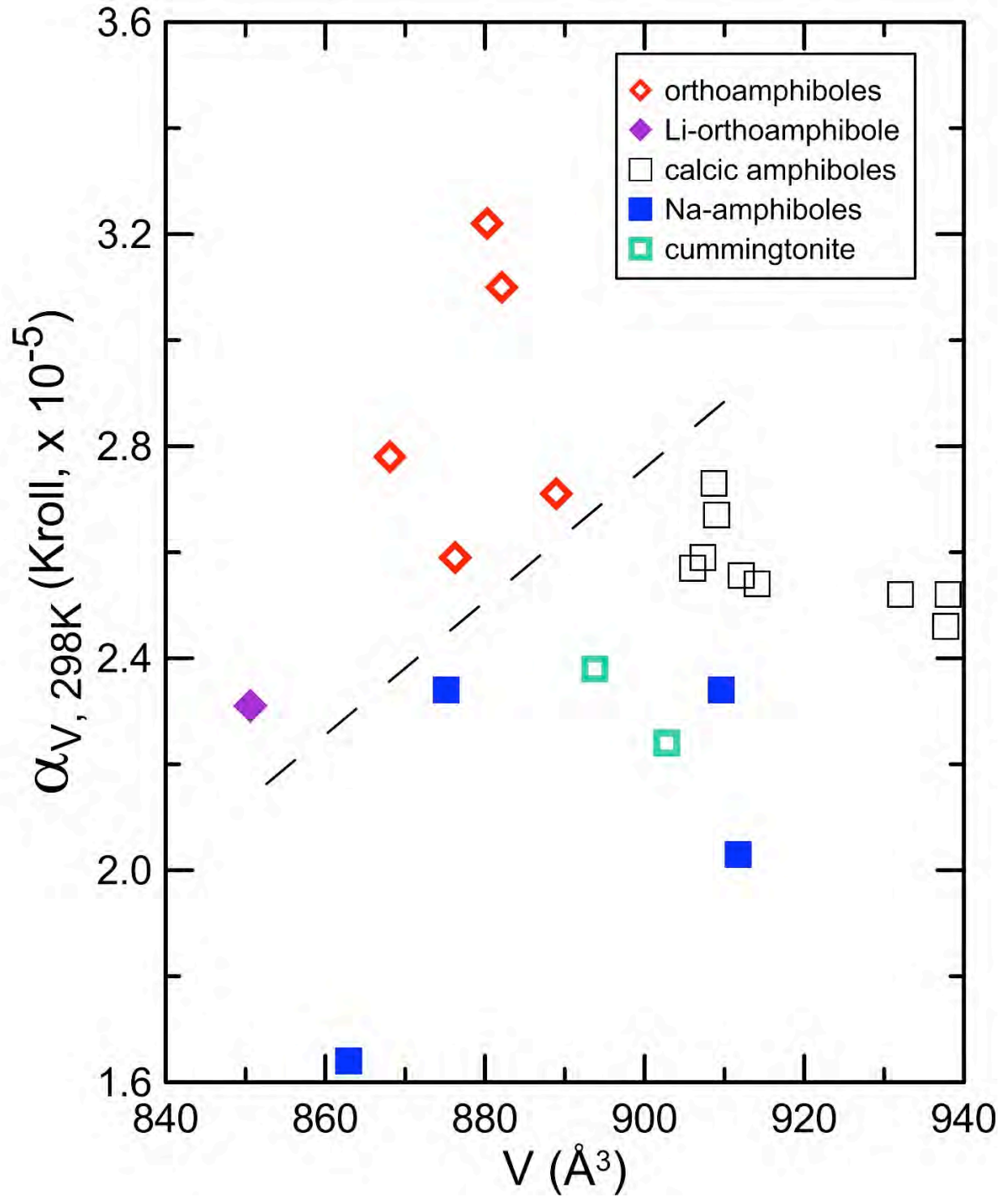


Figure 4

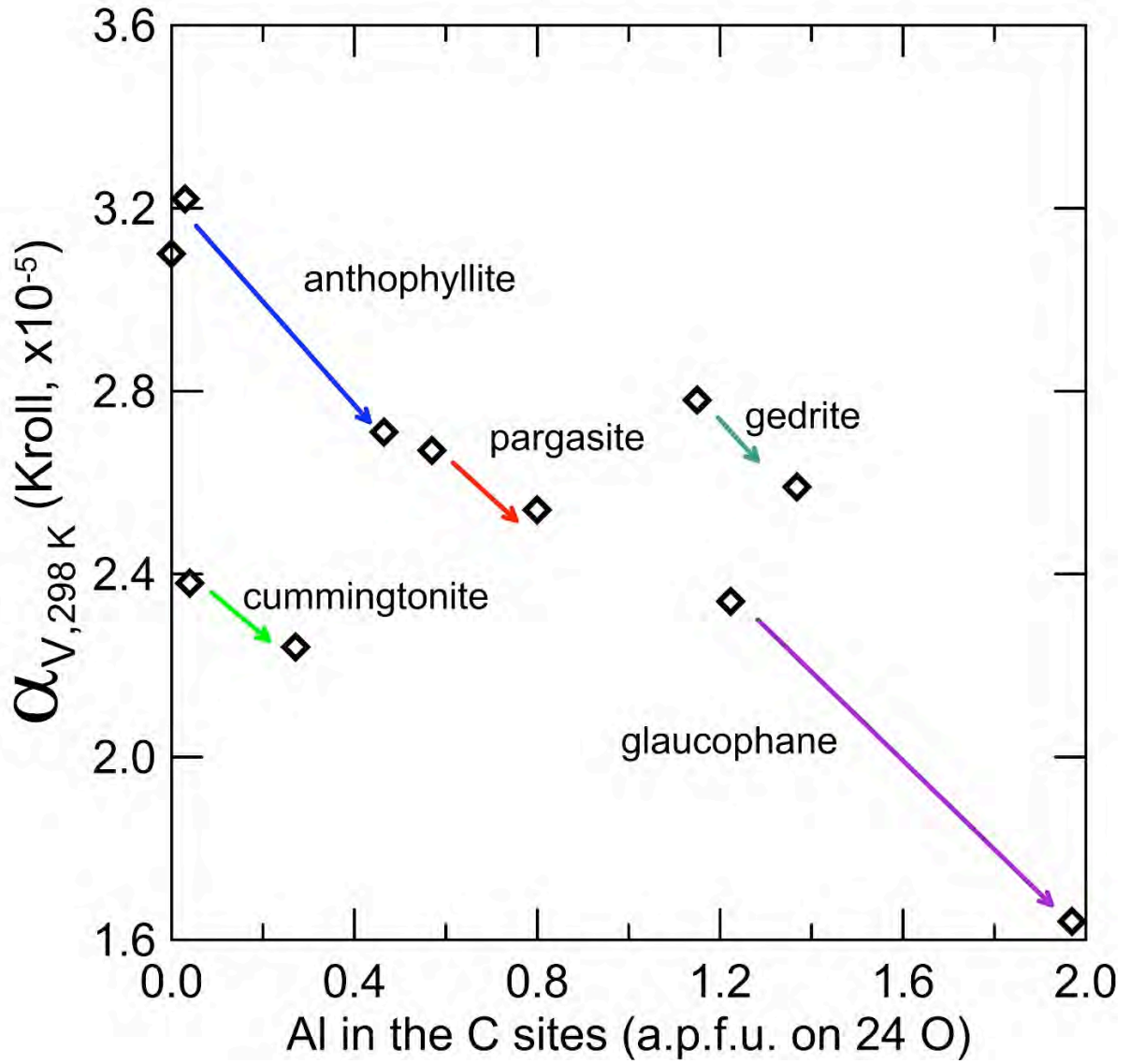


Figure 5

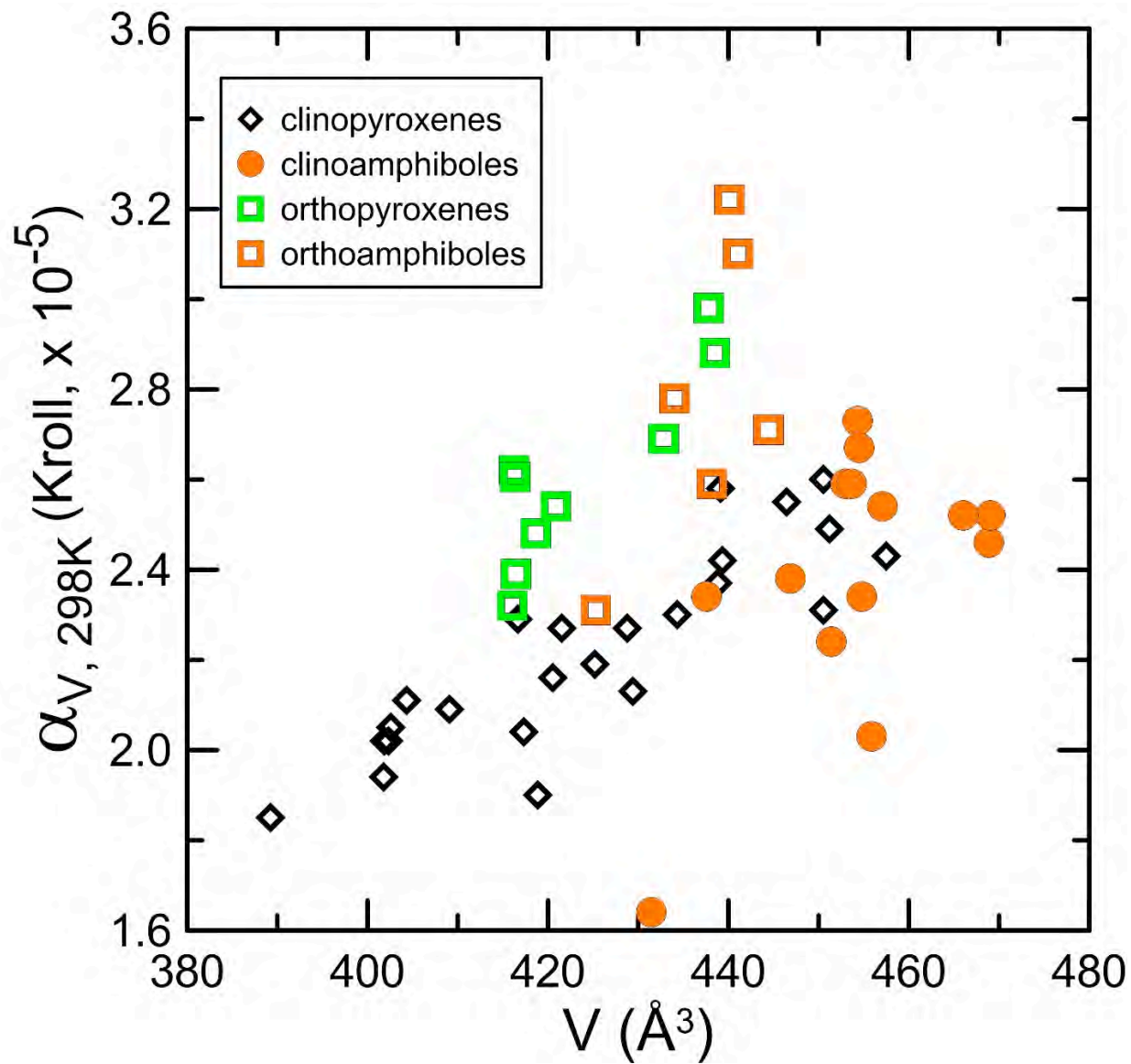


Figure 6

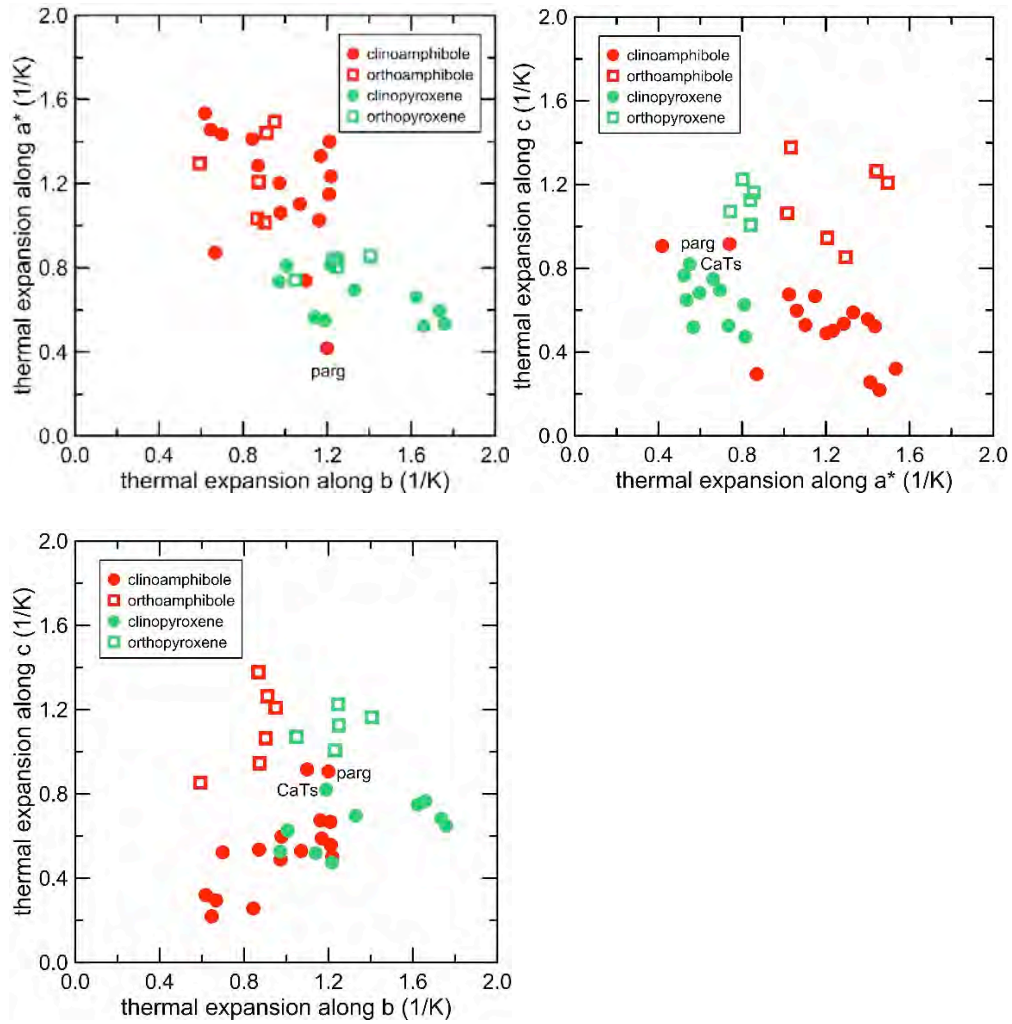


Figure 7

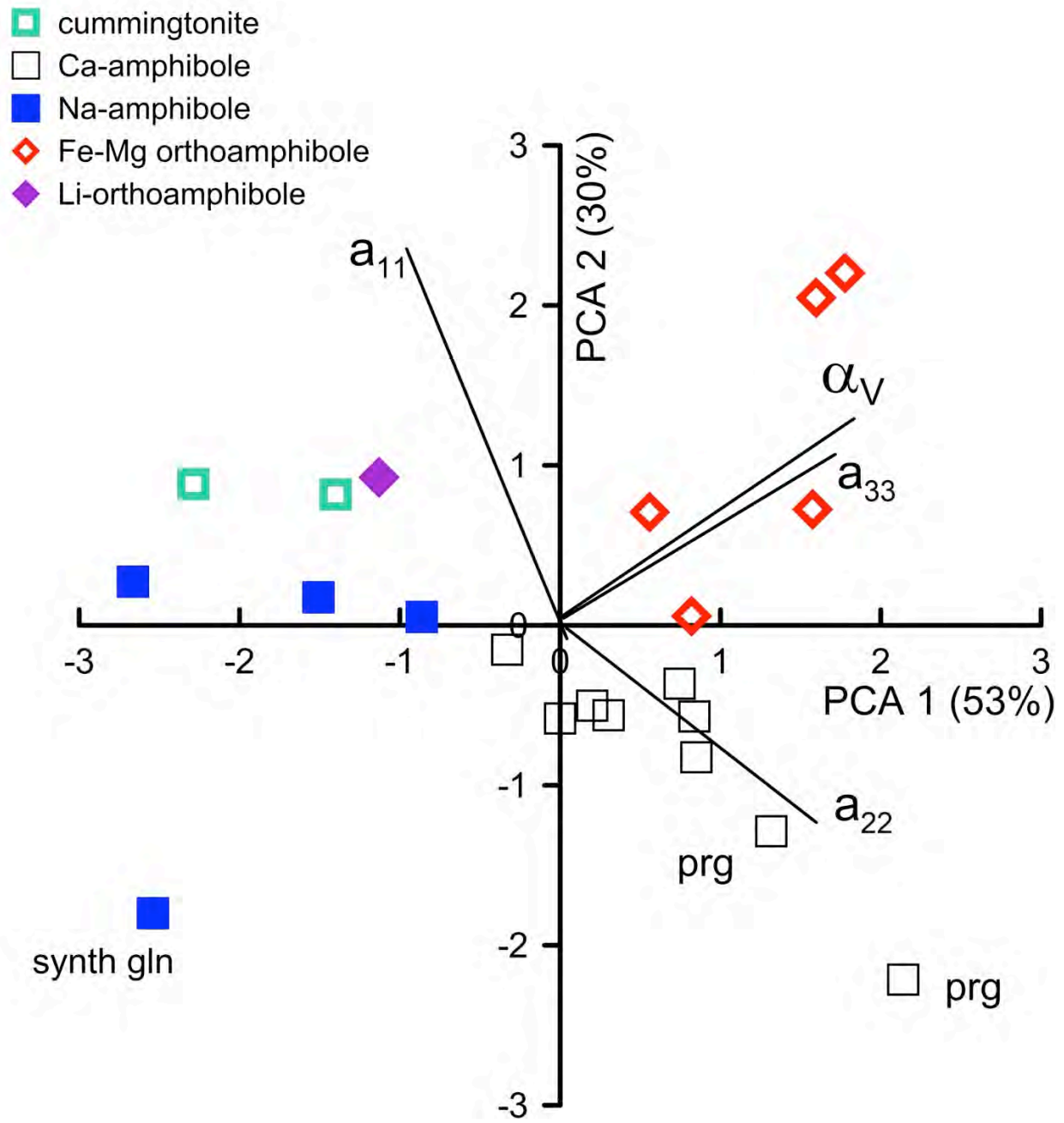


Figure 8

TABLE 1: Chemical and other information for the amphiboles investigated.

Final Name	Anthophyllite	Anthophyllite	Gedrite	Holmquistite	Cummingtonite
Catalogued name, source ¹ , and specimen	Anthophyllite AL 013/11 (also AMNH 18894)	Anthophyllite ² AL 003	Gedrite ² AL 016-3	Holmquistite ² AL ⁴ (no number)	Cummingtonite NMNH 118125
Locality	Saint-prejet-armandon, Haute-loire, Auvergne, France	Bancroft, Ontario, Canada	Orange area, Massachusetts, USA	Benson Mine, Mtoko, Southern Rhodesia	Bare Hills Copper Mine, Baltimore Co., Maryland
Relevant references and notes	Table 1a of Law (1989); Law and Whittaker (1981); M. Darby Dyar (pers. comm.); Fabries and Persei (1971)	Table 1a of Law (1989); Law and Whittaker (1981); M. Darby Dyar (pers. comm.); Tilley (1957)	Table 1a of Law (1989); Law and Whittaker (1981); M. Darby Dyar (pers. comm.); Robinson & Jaffe (1969), Papike & Ross (1970)	Analysis 1 in Table 1 of von Knorring and Hornung (1961)	NMNH, analysis of R. Rapp
Weight Percentages					
SiO ₂	54.86	49.18	39.66	59.06	55.28
TiO ₂	0.10	0.18	0.27	0.20	0.03
Al ₂ O ₃	2.52	7.14	19.26	12.38	0.26
Cr ₂ O ₃	0.00	0.00	0.00	0.00	0.03
MnO	0.09	0.57	0.24	0.25	0.57
FeO	5.63	18.08	18.75	10.84	20.02
Fe ₂ O ₃	1.83	0.91	1.17	2.36	0.00
MgO	30.34	18.08	13.46	8.82	20.05
CaO	1.08	0.83	0.25	0.21	0.63
Na ₂ O	0.00	0.74	1.88	0.11	0.04
K ₂ O	0.00	0.00	0.05	0.05	0.01
Li ₂ O	0.00	0.00	0.07	3.33	0.00
H ₂ O+	2.17	2.00	1.94	2.10	2.05
F	0.00	0.00	0.00	0.18	0.04
Cl	0.00	0.00	0.00	0.00	0.02
Total	100.00	100.00	100.00	99.88	99.03
Si ⁴⁺	7.534	7.352	6.079	7.887	8.000
Al	0.403	0.648	1.921	0.110	0.000
Ti	0.010	0.000	0.000	0.000	0.000
Sum T	7.947	8.000	8.000	7.997	8.000

Al	0.000	0.420	1.330	1.840	0.044
Ti	0.000	0.019	0.019	0.020	0.003
Cr	0.000	0.000	0.000	0.000	0.003
Fe ³⁺	0.190	0.136	0.000	0.237	0.225
Mg	4.864	4.047	3.051	1.756	4.326
Fe ²⁺	0.000	0.301	0.572	1.110	0.329
Mn	0.010	0.074	0.031	0.028	0.070
Sum C	5.064	4.996	5.002	4.991	5.000
Fe ²⁺	see footnote 4	1.839	1.939	0.100	1.869
Ca	0.000	0.092	0.021	0.030	0.098
Na	0.000	0.069	0.000	0.030	0.011
Li	0.000	0.000	0.040	1.790	0.000
Sum B	2.000	2.000	2.000	1.950	1.978
Ca	0.158	0.000	0.000	0.000	0.000
Na	0.000	0.130	0.586	0.000	0.000
K	0.000	0.000	0.000	0.000	0.002
Sum A	0.158	0.130	0.586	0.000	0.002
OH	1.990	1.963	1.962	1.883	1.751
F	0.000	0.000	0.000	0.077	0.018
Cl	0.000	0.000	0.000	0.000	0.005
O	0.010	0.037	0.038	0.040	0.226
sum W	2.000	2.000	2.000	2.000	2.000

1: AL = specimen of Anthony Law via M. Darby Dyar; AMNH = American Museum of Natural History

2: Monochromator utilized in the collection of designated amphibole XRD data.

3: UCLA specimen number reported as MS-2625 by Goldman (1979), but rather matches the local

4: $0.649 \text{ Fe}^{2+} + 1.351 \text{ Mg}^{2+}$

Grunerite	Tremolite	Ferro-actinolite	Tremolite	K-hastingsite	Pargasite
Cumingtonite e AMNH 24159	Tremolite NMNH 144178	Ferro-actinolite UCLA ^{2,3} MS-2825	Edenite NMNH R14496 ("Edenville tremolite")	Unnamed ² PBM-10	Pargasite NMNH 148884
Mikonui River, Westland, New Zealand	Gouvernor, St. Lawrence Co., NY	Biwabik Iron Formation, Babbitt, MN, USA	Edenville, Orange Co., NY, USA	Franklin, NJ, USA	Visakpapatram Dist., Andhra, Pradesh, India
AMNH microprobe analysis	Hawthorne and Grundy (1976)	Goldman (1979)	NMNH, microprobe analysis of D. Brabender and D. Jenkins	Microprobe analysis courtesy of M. Darby Dyar (Mount Holyoke College) and Molly McCanta (University of Tennessee)	Rao and Rao (1981)
52.90	56.57	48.61	57.06	40.27	42.05
0.06	0.01	0.00	0.08	1.25	0.76
2.37	1.41	1.86	1.45	8.06	15.86
0.00	0.00	0.00	0.00	0.00	0.12
0.97	0.03	2.22	0.04	0.31	0.21
28.00	0.08	30.27	1.32	29.67	8.35
0.00	0.01	0.00	0.00	0.00	2.36
13.71	24.41	3.83	22.92	3.21	14.18
0.55	12.25	10.59	12.06	10.53	10.98
0.00	1.44	0.26	1.16	1.68	2.52
0.00	0.68	0.15	0.44	1.99	0.83
0.00	0.00	0.00	0.00	0.00	0.00
1.04	1.46	1.88	0.52	1.83	1.28
0.00	1.52	0.00	0.85	0.00	0.08
0.00	0.05	0.04	0.03	0.00	0.00
99.60	99.92	99.71	98.47	98.80	99.58
7.856	7.771	7.705	7.880	6.498	6.078
0.144	0.228	0.295	0.120	1.502	1.922
0.000	0.001	0.000	0.000	0.000	0.000
8.000	8.000	8.000	8.000	8.000	8.000

0.271	0.000	0.052	0.116	0.030	0.780
0.007	0.000	0.000	0.008	0.152	0.083
0.000	0.000	0.000	0.000	0.000	0.014
0.054	0.010	0.000	0.030	0.785	0.257
3.035	4.999	0.905	4.719	0.773	3.055
1.511	0.000	3.810	0.122	3.218	0.812
0.122	0.003	0.300	0.005	0.042	0.026
5.000	5.012	5.067	5.000	5.000	5.026
1.912	0.012	0.202	0.000	0.000	0.198
0.088	1.803	1.798	1.784	1.821	1.704
0.000	0.185	0.000	0.216	0.179	0.076
0.000	0.000	0.000	0.000	0.000	0.000
2.000	2.000	2.000	2.000	2.000	1.978
0.000	0.000	0.000	0.000	0.000	0.000
0.000	0.199	0.080	0.095	0.346	0.630
0.000	0.119	0.030	0.078	0.410	0.153
0.000	0.318	0.110	0.173	0.756	0.783
1.805	1.328	1.990	1.622	1.432	1.963
0.000	0.660	0.000	0.371	0.106	0.037
0.000	0.012	0.010	0.007	0.326	0.000
0.195	0.000	0.000	0.000	0.138	0.000
2.000	2.000	2.000	2.000	2.002	2.000

History; NMNH = National Museum of Natural History; PBM = specimen of Paul B. Moore via
 ility for specimen MS-2825; analysis from Goldman (ibid).

Hastingsite	K-richterite	Glaucophane	Riebeckite
Hastingsite	Richterite	Glaucophane	Riebeckite
NMNH 95189	AMNH 39939	NMNH 138347	AMNH 35958
Stanley, Custer Co., Idaho, USA	McCloskey's Field, Quebec, Canada	Ile de Croix, France	St. Peter's Dome, Cheyenne District, El Paso, CO,
Shannon (1924)	AMNH, microprobe analysis of G. Harlow	NMNH, EPMA analysis by Y. Iizuka	AMNH, microprobe analysis of G. Harlow
38.50	56.98	56.00	51.10
0.00	0.00	0.00	0.41
10.88	0.38	7.80	0.93
0.00	0.00	0.00	0.00
0.00	0.13	0.20	1.35
27.28	2.40	13.80	24.31
6.70	4.42	0.00	10.12
1.40	20.23	10.30	0.13
11.30	5.72	1.90	0.13
1.22	5.09	6.40	8.20
1.66	2.61	0.00	1.42
0.00	0.00	0.00	0.00
1.86	2.15	3.60	1.90
0.00	0.00	0.00	0.00
0.00	0.00	0.00	0.00
100.80	100.11	100.00	100.00
6.191	7.962	7.922	8.000
1.809	0.038	0.078	0.000
0.000	0.000	0.000	0.000
8.000	8.000	8.000	8.000

0.253	0.025	1.223	0.173
0.000	0.000	0.000	0.048
0.000	0.000	0.000	0.000
0.811	0.455	0.421	1.198
0.336	4.214	2.172	0.030
3.602	0.290	1.212	3.197
0.000	0.015	0.024	0.180
5.002	5.000	5.051	4.826
0.066	0.000	0.051	0.000
1.934	0.856	0.288	0.000
0.053	1.144	1.661	2.000
0.000	0.000	0.000	0.000
2.000	2.000	2.000	2.000
0.013	0.000	0.000	0.021
0.000	0.235	0.095	0.502
0.327	0.465	0.000	0.284
0.341	0.701	0.095	0.807
2.000	2.000	2.000	1.904
0.000	0.000	0.000	0.000
0.000	0.000	0.000	0.000
0.000	0.000	0.000	0.096
2.000	2.000	2.000	2.000

M. Darby Dyar; UCLA collection, specimen of Bernard Evans via David Jenkins.

Table 2: Volume thermal expansion data (Kroll model).

Present Samples	Mineral	θ_D (K)	k'	$V_{0,298K}$ (\AA^3)	$\alpha_{V,298K}$ ($10^{-5}/K$)
Law 013/11	anthophyllite	447	4	1764.24 (17)	3.10 (2)
Law 003	anthophyllite	434	4	1777.87 (19)	2.71 (3)
Law 016-3	gedrite	456	4	1752.57 (1)	2.59 (1)
no number	holmquistite	501	4	1701.20 (20)	2.31 (4)
NMNH 144178	tremolite ¹	458	4	906.010 (7)	2.57 (1)
UCLA MS-2825	ferro-actinolite	362	4	932.12 (18)	2.52 (12)
NMNH R14496	Edenville tremolite	403	4	907.30 (5)	2.59 (2)
PBM 10	K-hastingsite	352	4	938.07 (4)	2.52 (3)
NMNH 118125	cummingtonite	426	4	893.77 (6)	2.38 (5)
AMNH 24159	grunerite	411	4	902.78 (5)	2.24 (3)
NMNH 148884	pargasite	391	4	914.11 (10)	2.54 (4)
AMNH 39939	K-richterite	401	4	908.69 (7)	2.73 (3)
AMNH 35958	riebeckite	399	4	909.59 (10)	2.34 (6)
NMNH 95189	hastingsite	351	4	937.72 (8)	2.46 (5)
NMNH 138347	glaucophane	458	4	875.15 (4)	2.34 (2)
Additional Samples					
Welch et al. (2011)	anthophyllite	447	4	1760.55 (10)	3.22 (2)
Zema et al. (2012)	gedrite	471	4	1736.16 (15)	2.78 (2)
Jenkins and Corona (2006)	glaucophane	479	4	862.93 (9)	1.64 (3)
Comboni et al. (2018)	pargasite	394	4	909.02 (4)	2.67 (1)
Tribaudino et al. (2008a)	richterite	356	4	912.12 (1)	2.59 (1)
Oberti et al. (2018)	riebeckite	395	4	911.72 (6)	2.03 (3)
1. Including Yang and Evans (1996) 140K datum.					

Table 3: Volume thermal expansion data (Fei model) .

Present Samples	Mineral	$V_{0,298\text{ K}} (\text{\AA}^3)$	$a_0 (\text{x}10^5)$	$a_1 (\text{x}10^8)$
Law 013/11	anthophyllite	1764.07 (25)	3.03 (29)	1.07 (53)
Law 003	anthophyllite	1777.74 (18)	2.3 (29)	1.70 (58)
Law 016-3	gedrite	1752.52 (3)	2.28 (13)	1.41 (27)
no number	holmquistite	1700.91 (14)	2.73 (3)	0
NMNH 144178	tremolite ¹	906.11 (8)	2.90 (12)	0.41 (15)
UCLA MS-2825	ferro-actinolite	932.07 (19)	2.71 (13)	0
NMNH R14496	Edenville tremolite	907.28 (7)	2.48 (15)	0.83 (28)
PBM 10	K-hastingsite	938.03 (4)	2.69 (3)	0
NMNH 118125	cummingtonite	893.83 (6)	1.98 (14)	1.34 (23)
AMNH 24159	grunerite	902.83 (7)	1.73 (27)	1.61 (59)
NMNH 148884	pargasite	913.95 (6)	2.85 (3)	0
AMNH 39939	K-richterite	908.53 (8)	3.06 (4)	0
AMNH 35958	riebeckite	909.53 (9)	2.56 (6)	0
NMNH 95189	hastingsite	937.68 (6)	2.64 (4)	0
NMNH 138347	glaucophane	875.22 (4)	1.71 (13)	1.94 (27)
Additional Samples				
Welch et al. (2011)	anthophyllite	1760.44 (17)	2.88 (19)	1.44 (34)
Zema et al. (2012)	gedrite	1735.89 (22)	2.85 (26)	0.80 (47)
Jenkins and Corona (2006)	glaucophane	863.06 (5)	0.92 (12)	1.84 (23)
Comboni et al. (2018)	pargasite	909.08 (5)	2.30 (10)	1.29 (18)
Oberti et al. (2018)	riebeckite	911.62 (6)	2.26 (3)	0
Tribaudino et al. (2008a)	richterite	912.11 (1)	2.83 (2)	0.27 (4)

1. Including Yang and Evans (1996) 140K datum.

a_2	$\alpha_{V, 298 K}$ ($10^{-5}/K$)
0	3.35
0	2.8
0	2.7
0	2.73
-0.33 (8)	2.65
0	2.71
0	2.72
0	2.69
0	2.38
0	2.21
0	2.85
0	3.06
0	2.56
0	2.64
0	2.29
0	3.31
0	3.09
0	1.47
0	2.68
0	2.26
-0.27 (1)	2.61

Table 4: Axial thermal expansion ($\times 10^{-5}$) and components of the strain ellipsoid in amphiboles. The expansion correspond to the a_{11} , a_{22} , a_{33} diagonal components of the strain ellipsoid in the Angel et al. (2018) model, that thermal expansion is here obtained from discrete steps between low temperature (LT) and high temperature (HT) cells, whereas the volume thermal expansion (Tables 2 and 3) is derived from the model as a first order approximation. The sign of ϵ_1 between ϵ_1 and a^* is positive when ϵ_1 is between $\underline{a^*}$ and \underline{c} , negative when between $\underline{a^*}$ and the negative

Source ¹	Clinoamphibole	LT-HT (°C)	α_{a^*}	α_b	α_c	$\epsilon_1 \sim a^*$
1	tremolite	25-516	1.15	1.21	0.67	1.24
1	tremolite	516-716	1.40	1.21	0.56	1.43
2	tremolite	25-700	1.33	1.17	0.59	1.37
1	ferro-actinolite	25-272	1.15	1.08	0.56	1.28
1	Edenville tremolite	25-516	1.10	1.07	0.53	1.19
1	K-hastingsite	25-322	1.20	0.94	0.49	1.20
1	cummingtonite	25-522	1.43	0.70	0.52	1.61
1	grunerite	25-522	1.53	0.62	0.32	1.68
1	pargasite	25-516	0.74	1.10	0.92	0.47
3	pargasite	25-773	0.42	1.20	0.91	0.22
1	K-richterite	25-516	1.23	1.22	0.50	1.24
4	richterite	25-600	1.02	1.18	0.67	1.22
1	riebeckite	25-316	1.41	0.84	0.26	1.42
5	riebeckite	25-598	1.46	0.65	0.22	1.46
1	hastingsite	25-316	1.06	0.98	0.60	1.11
1	glaucophane	25-466	1.29	0.87	0.53	1.29
6	glaucophane	25-500	0.87	0.67	0.29	0.84
	Orthoamphibole		$\epsilon_1 \equiv a$	$\epsilon_2 \equiv b$	$\epsilon_3 \equiv c$	
1	anthophyllite 013/11	25-522	1.44	0.91	1.26	
7	anthophyllite	25-525	1.49	0.95	1.21	
1	anthophyllite 003	25-522	1.21	0.87	0.95	
1	gedrite	25-422	1.01	0.9	1.06	
8	gedrite	25-400	1.03	0.87	1.38	
1	holmquistite	25-472	1.3	0.59	0.85	

1. Data from 1: this work; 2: Sueno et al. (1973); 3: Comboni et al. (2018); 4: Tribaudino et al. (2018); 5: Tribaudino et al. (2018); 6: Jenkins and Corona (2006); 7: Welch et al. (2011); 8: Zema et al. (2012).

the α_{a^*} , α_b and α_c axial
t al. (2014) notation. Note
h temperature (HT) unit
derivative. The angle
tive of c .

$\epsilon_3 \sim c$	$\epsilon_1 \wedge a^* (\circ)$
0.58	21.6
0.53	10.1
0.55	12
0.44	22.5
0.44	19.7
0.42	17.7
0.35	21.7
0.17	18.2
1.19	-37.9
1.10	-28.2
0.50	5.1
0.51	27.6
0.25	5.3
0.21	-3.2
0.55	16.8
0.53	5.2
0.28	-9.5

08); 5: Oberti et al.
